Driven inertial oscillations in spherical shells

A. Tilgner
Institute of Physics, University of Bayreuth, D-95440 Bayreuth, Germany
(Received 24 August 1998)

The flow of a fluid in a rapidly rotating spherical shell whose rotation rate is modulated sinusoidally in time is simulated numerically. Different inertial modes are excited as the modulation frequency is varied. The inertial modes are structured by internal layers. Internal layers are reflected at the boundaries such that at certain modulation frequencies, the layers are focused onto ''attractors'' after multiple reflections. The geometric properties of these attractors and their relevance for the response of the fluid is investigated. [S1063-651X(99)06402-8]

PACS number(s): 47.35.+i, 47.10.+g, 47.52.+j

I. INTRODUCTION

Both rotating and stably stratified fluids are capable of oscillatory motion; inertial oscillations in the first case and internal gravity waves in the second. It has recently been shown by Maas and Lam [1] that rays of internal waves propagating in irregularly shaped basins tend to be focused onto an ''attractor.'' The focusing effect arises from the peculiar reflection law of internal gravity waves at solid walls: the angle of the wave vector with the direction of gravity is conserved during reflection, rather than the angle formed with the normal to the reflecting surface. Unlike the situation met with billiards considered in quantum chaos, attractors of internal gravity waves are associated with negative Lyapunov exponents. It was surmised later on [2] that the response of a stably stratified or rotating fluid to external forcing should be determined by the geometrical properties of these attractors. In particular, the spectral width of resonances might be determined by the size of the interval of frequencies in which certain attractors exist. Maas *et al.* [2] suggest that past experiments on inertial oscillations in variously shaped containers may be interpreted in terms of attractors. Similar ideas have been expressed before, e.g., by Bretherton [3] and Israeli [4], who considered modes trapped near the equator of a spherical shell with wave packets traveling along a closed circuit.

The present paper intends to test some of the ideas advanced in Ref. [2] in the context of a rapidly rotating spherical shell. The ray properties leading to attractors are strictly obtained only for inviscid fluids. Here, numerical simulations are presented which include viscosity in order to study its influence on the existence of attractors. The simulated flow is much the same as one which had been studied experimentally before [5,6]: The rotation rate of the shell is varied sinusoidally in time at a given frequency. Spectroscopy of the shell is performed by sweeping the modulation frequency. Numerical simulations allow us to compare the excited flows with previously computed eigenmodes and to assess the role of ray attractors.

Inertial modes in rapidly rotating fluids are also of interest in connection with several geophysical problems. It has been claimed that such modes in the liquid outer core have been detected with superconducting gravimeters following strong earthquakes [7]. Inertial modes are also a useful starting point to describe some instabilities: Convection at low Prandtl number can be viewed as inertial oscillations perturbed by buoyancy [8,9] and precessing flows may become unstable through triad interactions between inertial modes [10]. While inertial modes in spheres can be handled analytically, much less is known about these oscillations in ellipsoidal or even spherical shells. Rieutord and Valdettaro [11] studied some of the least damped modes in spherical shells and demonstrated the appearance of internal shear layers. The geophysical application motivates study of a spherical shell (as opposed to other container shapes) and in particular a shell with a ratio of inner to outer radius near 0.35 which approximates the geometry of the earth's core.

After the mathematical model and numerical methods are introduced in Sec. II, ray propagation is studied in Sec. III. The relation between ideal rays and real internal layers is investigated in Sec. IV, whereas Sec. V investigates inertial mode spectra and how spectra are influenced by the concentration of kinetic energy on internal layers in the excited flows.

II. MATHEMATICAL FORMULATION OF THE PROBLEM AND NUMERICAL METHODS

A spherical shell of gap d filled with fluid of viscosity ν rotates about the z axis with angular velocity $\Omega_0 + \Omega_1 \cos\tilde{\omega}t$. Using for units of time and length $1/\Omega_0$ and d, respectively, one obtains in the frame rotating at the rate Ω_0 about the z axis the nondimensional equation of motion

$$\frac{\partial}{\partial t}\boldsymbol{v} + 2\hat{\boldsymbol{z}}\times\boldsymbol{v} = -\nabla p + E\nabla^2\boldsymbol{v}, \quad \nabla\cdot\boldsymbol{v} = 0, \tag{1}$$

where E is the Ekman number defined by $E=\nu/\Omega_0 d^2$ and p is a reduced pressure. The no-slip boundary conditions require for the fluid velocity $\boldsymbol{v}$ that $\boldsymbol{v}=(\Omega_1/\Omega_0)\cos(\omega t)\hat{\boldsymbol{z}}\times\boldsymbol{r}$ at the inner and outer boundaries of radii r_i and r_0 with $r_0 - r_i = 1$ and $\omega=\tilde{\omega}/\Omega_0$. Since the study of ''modes'' presupposes linear dynamics, the nonlinear term has been dropped from the Navier-Stokes equation and Ω_1/Ω_0 is arbitrarily set equal to 1.

Temporal and spatial dependences can be separated by the ansatz $\boldsymbol{v}=\mathrm{Re}\{\boldsymbol{u}(\boldsymbol{r})e^{i\omega t}\}$, where Re denotes the real part. $\boldsymbol{u}$ is decomposed using poloidal and toroidal scalars Φ and Ψ:

$$\boldsymbol{u}=\nabla\times\nabla\times(\Phi\hat{\boldsymbol{r}})+\nabla\times(\Psi\hat{\boldsymbol{r}}). \tag{2}$$

Only axisymmetric flow is excited by the driving mechanism considered here so that Φ and Ψ can be decomposed into radial and angular parts using Legendre polynomials P_l in spherical polar coordinates (r,θ,φ):

$$\Phi=r\sum_{l=1}^{\infty}V_l(r)P_l(\cos\theta),\quad \Psi=r^2\sum_{l=1}^{\infty}W_l(r)P_l(\cos\theta). \tag{3}$$

Operating with $\hat{\boldsymbol{r}}\cdot\nabla\times$ and $\hat{\boldsymbol{r}}\cdot\nabla\times\nabla\times$ on Eq. (1), one obtains

$$\begin{aligned} &i\omega\mathcal{D}_lV_l-E\cdot\mathcal{D}_l^2V_l\\ &\quad=2\left\{-\frac{(l+2)(l+3)}{2l+3}W_{l+1}-\frac{l+2}{2l+3}r\frac{dW_{l+1}}{dr}\right.\\ &\qquad\left.+\frac{(l-1)(l-2)}{2l-1}W_{l-1}-\frac{l-1}{2l-1}r\frac{dW_{l-1}}{dr}\right\}, \end{aligned} \tag{4}$$

$$\begin{aligned} &i\omega W_l-E\left(\frac{d^2}{dr^2}+\frac{4}{r}\frac{d}{dr}+\frac{2-l(l+1)}{r^2}\right)W_l\\ &\quad=\frac{2}{r^2}\left\{\frac{(l+2)^2}{2l+3}V_{l+1}+\frac{l+2}{2l+3}r\frac{dV_{l+1}}{dr}\right.\\ &\qquad\left.-\frac{(l-1)^2}{2l-1}V_{l-1}+\frac{l-1}{2l-1}r\frac{dV_{l-1}}{dr}\right\} \end{aligned} \tag{5}$$

with $\mathcal{D}_l=d^2/dr^2+(2/r)(d/dr)-l(l+1)/r^2$. Equations (4) and (5) need to be solved subject to the boundary conditions

$$V_l=\frac{dV_l}{dr}=0,\quad W_l=\delta_{1,l}\quad \text{at } r=r_i,r_0. \tag{6}$$

Equations (4) and (5) still need to be discretized in radius. To this end, V_l and W_l are expanded in n_r Chebychev polynomials T_n as

$$V_l(r)=\sum_{n=0}^{n_r-1}v_{l,n}T_n(x),\quad W_l(r)=\sum_{n=0}^{n_r-1}w_{l,n}T_n(x) \tag{7}$$

with $-1\leqslant x\leqslant 1$ and the dependence of r on x yet to be chosen. Equations (4) and (5) are converted into a set of algebraic equations by the collocation method, i.e., by enforcing Eqs. (4) and (5) at certain collocation points, and by truncating the sums in Eq. (3) at some L to retain only Legendre polynomials with $l\leqslant L$. Boundary conditions are enforced by replacing the dynamic equations at the collocation points on or next to the boundaries. A detailed description of the discretization scheme and the treatment of boundary conditions can be found in Ref. [12].

A popular choice of collocation points x_n and r_n with Chebychev polynomials is

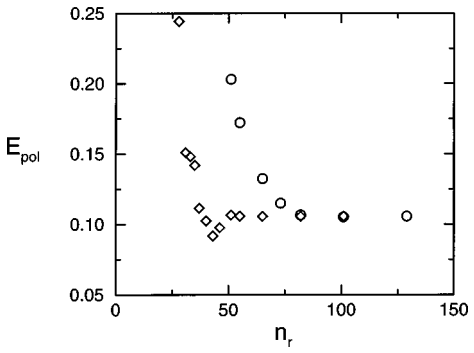

FIG. 1. Poloidal energy E_{pol} of a fluid in a shell with $r_i/r_0=0.35$ driven at $\omega=0.633$ and $E=10^{-6}$. E_{pol} is computed with 128 Legendre and n_r Chebychev polynomials using $\beta=0$ (circles) and $\beta=0.9$ (diamonds).

$$x_n=\cos\left(\pi\frac{n-1}{n_r-1}\right),\quad r_n=r_i+\frac{x_n+1}{2},\quad n=1,\ldots,n_r. \tag{8}$$

This choice allows one the use of fast transforms to convert between direct space and Chebychev coefficients when setting up the matrix. In the present application, it is important to resolve the thin Ekman layers and to crowd collocation points near the boundaries. This is achieved (yet keeping the possibility of using fast transforms) by stretching the radial coordinate as follows:

$$\begin{aligned} &x_n=\cos\left(\pi\frac{n-1}{n_r-1}\right),\quad r_n=r_i+\frac{1}{2}\left(\frac{\sin(\beta\pi x_n/2)}{\sin(\beta\pi/2)}+1\right),\\ &\qquad 0<\beta<1,\quad n=1,\ldots,n_r. \end{aligned} \tag{9}$$

The restriction on β ensures invertibility of $r(x)$, the limit $\beta\to 0$ recovers the traditional Chebychev collocation points (8). β can be optimized to ensure fast convergence: As an example, Fig. 1 compares the poloidal energies E_{pol} obtained with $\beta=0$ and $\beta=0.9$ for $r_i/r_0=0.35$, $E=10^{-6}$, $\omega=0.633$, and $L=128$. E_{pol} is computed as

$$E_{\mathrm{pol}}=2\pi\int_{r_i}^{r_0}\sum_{l=1}^{L}\frac{l(l+1)}{2l+1}\left(l(l+1)|V_l|^2+\left|r\frac{dV_l}{dr}+V_l\right|^2\right)dr. \tag{10}$$

It is seen in Fig. 1 that results converge much faster with an appropriate distribution of collocation points. Further details on convergence properties are given in Table I.

The highest resolution used in this work was $n_r=161$, $L=200$ (e.g., in Fig. 8). Typical spectra were obtained with $n_r=82$ and $L=128$ (all with $\beta=0.9$). The experience accumulated in the course of this work is that better resolution is necessary for a given accuracy with increasing frequency because the oscillatory Ekman layers become thinner. The structure of the flow is, however, well reproduced by poorly resolved computations even if they yield a poloidal energy in error by a factor of 4 or more. Also, the location of spectral lines is accurate for such underresolved runs. In the spectrum for $E=10^{-7}$ in Fig. 9, the estimated error in the poloidal energy increases with frequency to reach about 30% at the highest frequency, whereas the error stays below 5% for E

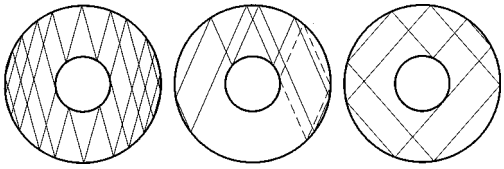

FIG. 2. Ray attractors in a shell with $r_i/r_0=0.35$ for $\omega=0.532$ (left), $\omega=0.81$ (center, the dashed line indicates a second attractor), and $\omega=1.322$ (right). The rotation axis is vertical in this figure.

$=10^{-6}$. No effort has been made to improve the situation at $E=10^{-7}$ because of the computational burden that would ensue and because the main interest was in locating resonant frequencies rather than obtaining precise amplitudes.

The driving mechanism under study excites modes which are symmetric about the z axis and the equator. It follows that only V_l with l even and W_l with l odd are different from zero. If the nonzero $v_{l,n}$ and $w_{l,n}$ are appropriately arranged in a single vector, the matrix representing Eqs. (4) and (5) becomes block-tridiagonal. The system of equations can then be solved with standard methods of LU decomposition and backsubstitution formulated for banded matrices.

The code has been validated by comparing resonant flows and frequencies of a shell with $r_i/r_0=0.01$ with the eigenmodes of a full sphere [13] and by comparing results for $r_i/r_0=0.35$ with eigenmodes obtained in [14].

III. RAY GEOMETRY

In an inviscid unbounded fluid, inertial waves of wave vector $\boldsymbol{k}$ have the angular frequency $\omega=\pm 2|\boldsymbol{k}\cdot\hat{\boldsymbol{z}}|/|\boldsymbol{k}|$, independent of $|\boldsymbol{k}|$ [13]. The group velocity is perpendicular to the phase velocity and directed along the characteristics of Eq. (4) for $E=0$. The characteristics form the angle ϑ_r with the z axis such that $\tan\vartheta_r=\pm(4/\omega^2-1)^{-1/2}$. Waves excited at the angular frequency ω can therefore superpose to form rays inclined at angle ϑ_r. Singularities may also develop on the characteristics in time periodic inviscid flows. In a spherical shell, characteristics are tangent to boundaries at ''critical'' latitudes ϑ_c with $\tan\vartheta_c=\pm(4/\omega^2-1)^{-1/2}$.

When a ray crosses a boundary, it is reflected such that the angle enclosed with the rotation axis remains unchanged (see Fig. 2). This unusual reflection law opens the possibility for rays to converge to ''caustics,'' ''limit cycles,'' or ''attractors'' after multiple reflection. This process is demonstrated in Fig. 3. A ray has been started in poleward direction from the inner sphere at northern critical latitude and reflected 1500 times on the boundaries of a spherical shell with $r_i/r_0=0.35$. For the next 500 reflections, a dot is placed in Fig. 3 at the colatitude θ at which a reflection off the outer boundary occurs. This procedure is repeated for different ω with a step size $\Delta\omega=0.002$. For some ω the ray path covers more or less the entire shell, whereas for other ω, the ray reaches a periodic orbit. Examples of simple attractors are shown in Fig. 2.

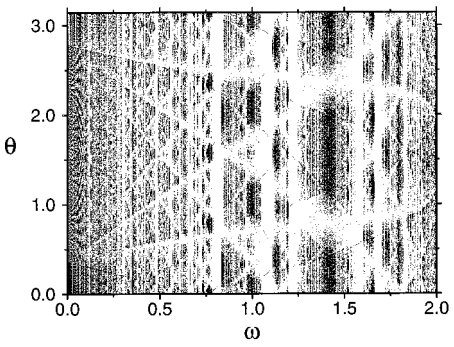

FIG. 3. Ray reflections on the outer sphere at colatitude θ as a function of ω (see text).

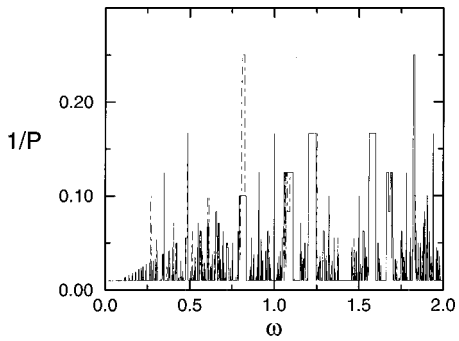

FIG. 4. $1/P$, with P the period of an attractor, as a function of ω for a shell with $r_i/r_0=0.35$. Periods larger than 100 have not been determined and are set to 100 in this plot. The period of an attractor found by starting a ray from critical latitude at the inner sphere towards the pole (equator) is indicated with the continuous (dot-dashed) line.

The main properties of the attractors are summarized in Figs. 4 and 5. In Fig. 4, the period P of the orbits is evaluated by counting the number of reflections after which the ray returns to a position it had passed previously. The figure contains two curves because two independent attractors (which cannot be transformed into each other by a symmetry operation) coexist in a spherical shell at some frequencies (see Fig. 2). These attractors have been found by starting rays from the inner sphere at critical latitude in the direction towards the pole or the equator. A case with three coexisting attractors has been searched for by starting rays from arbitrary positions but no example could be found. Figure 5 shows a Lyapunov exponent λ defined by

$$\lambda=\frac{1}{N}\sum_{n=1}^{N}\ln\left|\frac{d\theta_{n+1}(\theta_n)}{d\theta_n}\right|, \tag{11}$$

TABLE I. Poloidal energy $E_{\rm pol}$ computed for $r_i/r_0=0.35$, $E=10^{-6}$ and $\omega=0.633$ using a resolution of n_r Chebychev and L Legendre polynomials. Collocation points are distributed with $\beta=0.9$.

n_r	L	$E_{\rm pol}$
33	128	0.1482
65	32	0.0898
65	64	0.1020
65	128	0.1058
65	256	0.1054
82	128	0.1058
82	256	0.1056

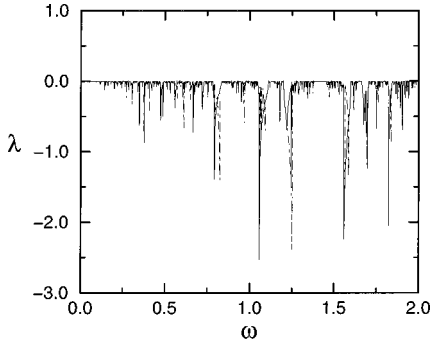

FIG. 5. Lyapunov exponent λ as a function of ω for a shell with $r_i/r_0=0.35$. The meaning of continuous and dot-dashed traces is the same as in Fig. 4.

where θ_n measures the colatitude of the nth reflection off the outer boundary and N is a large number (e.g., 500). The sum in Eq. (11) is computed for a ray which has already experienced a large number of reflections (e.g., 1500). λ is mostly negative and never large when it is positive, which justifies the use of the word ''attractor.''

Some simple periodic cycles may actually be missed in plots like Fig. 4. For instance, there is a trivial cycle of period 4 at $\omega=\sqrt{2}$ which does not show up in Fig. 4 because $\sqrt{2}$ falls in between the values of ω for which the period has been evaluated.

The property of focusing rays onto attractors is a common feature of spherical shells. The Lyapunov exponents for a different shell ($r_i/r_0=0.8$) are given in Fig. 6. Attractors do not exist in a full sphere and become rare in shells with small cores because the probability of a ray hitting the core decreases and rays are seldom deflected from the path they would follow in a full sphere.

IV. FLOW STRUCTURE

The most conspicuous feature of the flows to be described in this section are internal layers in which the kinetic energy density reaches a local maximum. These layers may be regarded as viscously broadened singularities of an inviscid solution and obey the reflection law discussed above. If internal layers can be approximated by rays at small E, one would expect (at low enough E and at frequencies at which attractors exist) to find internal layers at the location of the attractor, because where else could these layers survive if they end up on the attractor after multiple reflections? When comparing plots of simulated flows (Figs. 7 and 8) with attractors, bear in mind that the flows are axisymmetric and that the attractors in Fig. 2 can also be reflected about the equator to yield additional attractors.

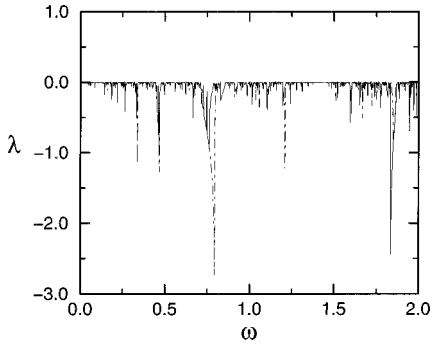

FIG. 6. Same as Fig. 5 with $r_i/r_0=0.8$.

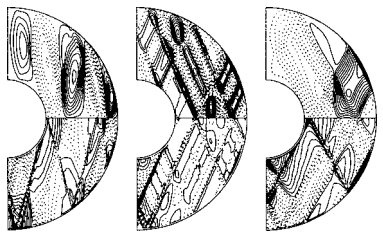

FIG. 7. Flow patterns in a shell with $r_i/r_0=0.35$ driven at $\omega=0.532$, $E=10^{-6}$ (left); $\omega=0.81$, $E=10^{-7}$ (center); and $\omega=0.9474$, $E=10^{-6}$ (right). The upper half of each panel shows meridional streamlines [contour lines of $-\Sigma_l \mathrm{Re}(V_l e^{i\omega t}) r \sin\theta\, dP_l/d\theta$], the lower half azimuthal velocity u_φ. The Ekman layers have been removed from the plots of u_φ for clarity. Continuous lines correspond to positive values, dashed lines to negative values. Streamlines are shown at a time at which the instantaneous poloidal energy is maximum, u_φ is shown a quarter cycle of the driving force earlier. The rotation axis is vertical in this figure.

The simulations show that the internal layers in driven flows are indeed located on a predicted attractor if its period is small (10 or less). The frequencies at which periods change in Fig. 4 do not always coincide precisely with a change in morphology of the flow. The simple pattern of internal layers at $\omega=1.32$ (Fig. 8) corresponds best to the attractor at $\omega=1.322$ (Fig. 2) but not to the one at exactly $\omega=1.32$ (see also the examples given in [11]). The comparison is still lacking in this case because the pattern at $\omega=1.32$ is equator symmetric whereas the attractor at $\omega=1.322$ is not.

However, the main difference with the attractor shapes is that the pattern of internal layers may remain connected to the critical latitudes where rays are tangent to the inner core. $\omega=0.532$ and $\omega=0.9474$ (Fig. 7) provide examples of rays which emanate from critical latitudes and dissipate away before they reach an attractor because of too many reflections or because they propagate close to a boundary. Attractors at nearby values of ω have a large period (>28) and do not appear in the actual flows.

The special role of the critical latitudes leads, on the other hand, to simple patterns for some ω at which no attractor with a clearly negative λ exists. At $\omega=\sqrt{2}$, for instance, internal layers appear on a rectangle inclined at 45° with respect to the z axis with two sides tangent to the inner core. This pattern is of course a periodic cycle for rays, but it is not an attractor in the sense that a nearby ray will not be focused on this particular rectangle (infinitely many neighboring rectangles are also closed cycles for rays). Another example is the nonaxisymmetric flow excited by precession ($\omega=1$). A ray started from the inner sphere at critical latitude in a shell with $r_i/r_0=0.35$ runs in a closed cycle which is not an attractor. This pattern is nevertheless observed in the spin over mode [15] and simulations of precession driven flows [16].

It has been noted by many authors that the Ekman layers break down and spawn internal shear layers at critical latitudes. However, the structure of the flow driven at $\omega=0.9474$ with free slip boundary conditions on the inner

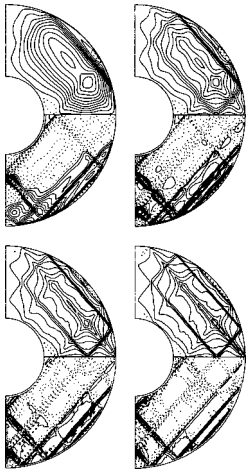

FIG. 8. Same as Fig. 7 for $\omega=1.32$ and Ekman numbers 10^{-5} (top left), 10^{-6} (top right), 10^{-7} (bottom left), and 10^{-8} (bottom right).

sphere cannot be visually distinguished from the corresponding plot in Fig. 7 except for a missing Ekman layer. Similar observations are reported in [17]. The special role of the critical latitudes and the structure of internal layers is not necessarily determined by a no-slip surface. Stewartson and Rickard [18] even found discontinuities tangential to the inner sphere in *inviscid* inertial modes of a spherical shell. Note that internal layers seem to be absent from the eigenmodes obtained in Refs. [8,9] which are localized near the outer surface and are little influenced by the presence of an inner core.

Another curiosity shows up at $\omega=0.81$ (Fig. 7). A ray may start from the north pole of the inner core, reflect once from the outer boundary in the northern hemisphere, and a second time in the southern hemisphere such that the ray returns exactly upon itself. Such a closed circuit exists for ideal rays at an ω near 0.8324 for $r_i/r_0=0.35$ and is again not an attractor, but it appears in the flow shown in Fig. 7.

The Ekman numbers within reach of today's computers are still many orders of magnitude above the Earth's estimated Ekman number (10^{-15}). Figure 8 presents a study of the Ekman number dependence at $\omega=1.32$. The internal layers narrow with decreasing E but do not seem to converge to ideal rays: In the poloidal component, the number of streamlines lying outside of what is perceived as a region of large velocity remains constant from $E=10^{-6}$ to 10^{-8}. Deviations of internal layers from an ideal ray are a source of discrepancy between the attractor picture and real flows.

Several unfruitful attempts have been made to excite trapped modes of short wavelength as envisioned by Bretherton [3]. Figure 2 shows an example of a trapped attractor at $\omega=0.81$, but another attractor extending to the poles also exists at the same ω. The trapped attractor is hardly excited in Fig. 7. The boundary conditions have then been changed so that the shell (or only the inner or only the outer sphere) moves only within a narrow strip around the latitudes visited by the trapped ray pattern. Various frequencies and shell geometries have also been tried in which trapped attractors pass through critical latitudes. In all cases, the intensity of layers in the polar region was at least comparable to the intensity of layers near the equator. The layers in these flows

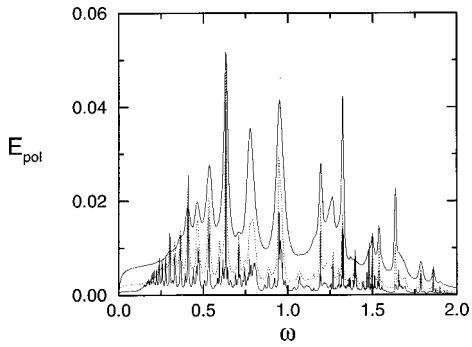

FIG. 9. Poloidal energy spectra for a shell with $r_i/r_0=0.35$ at Ekman numbers 10^{-5} (upper continuous trace), 10^{-6} (dashed line), and 10^{-7} (lower continuous trace).

are not rays of infinitesimal width and some energy always escapes from the trapped attractor to excite other, global modes. Because modes of the Bretherton type must be strongly damped, they do not dominate in amplitude other extended, less damped modes which also contain internal layers and are inevitably excited, too.

V. SPECTRA

The poloidal energy is chosen throughout this section as the representative quantity to measure the response of the fluid. The toroidal energy reveals essentially identical spectra with an additional peak at $\omega=0$. The frequencies chosen as examples in previous figures correspond to resonances of the fluid. In experiments [5,6], spectra of pressure differences are measured. Comparison of linear theory with experiment has been made by Rieutord [19] and will not be repeated here.

The first observation about the spectra in Fig. 9 is that no obvious connection exists between the spectral response and the attractor geometry as quantified by the period or Lyapunov exponent, although rays are very prominent in the structure of the excited flows. Upon decreasing E, spectral lines narrow and become more numerous to emerge from the background. Theory predicts that linewidths and frequency displacements due to variation of E are of order $E^{1/2}$. These predictions are compatible with Fig. 9 but cannot be put to serious test because spectral lines often contain the response of several modes. However, there is no indication that the width of the lines is limited by the characteristic spectral width of the geometric properties of ray attractors in Fig. 4.

The height of some peaks decreases dramatically with decreasing E, e.g., at $\omega=0.78$, 1.32, or 1.63. The amplitude A of the fluid response is given to $O(E^{1/2})$ by equation 2.14.8 of Ref. [13]. Apart from frequency and Ekman number independent factors, the expression for A near resonance with a mode with eigenvalue $\omega_0+iE^{1/2}s$ and $|E^{1/2}s|\ll\omega_0$ simplifies to

$$A\propto\left(1-\frac{\omega_0^2}{4}\right)\frac{\omega_0^2}{2}\,\frac{E^{1/2}}{\Delta\omega-iE^{1/2}s}, \tag{12}$$

where $\Delta\omega$ is the detuning $\omega-\omega_0$. Exactly at resonance, A is independent of E. The height of a peak in the spectrum (measured from the background level to which many modes con-

tribute) must therefore not depend on E if the spectral line contains a single mode. The situation is different for a multiple line. Take the example of two modes $\boldsymbol{u}_1$ and $\boldsymbol{u}_2$ resonant at ω_1 and ω_2, driven at ω, and excited with amplitudes $A_1(\omega)$ and $A_2(\omega)$. The kinetic energy contained in the flow is given by the volume integral $\int|A_1(\omega)\boldsymbol{u}_1+A_2(\omega)\boldsymbol{u}_2|^2dV$. Inviscid inertial modes are exactly orthogonal to each other (in the sense of $\int\boldsymbol{u}_1^*\cdot\boldsymbol{u}_2dV=0$[13]), and modes at small E are still nearly orthogonal. The total kinetic energy is thus approximately given by $\epsilon_1(\omega)+\epsilon_2(\omega)$, where ϵ_1 and ϵ_2 are the energies of both modes taken individually. For, say, $\omega=\omega_1$, the excited energy is independent of E if there is no spectral overlap with the line due to the second mode. Otherwise, the energy in the fluid driven at ω_1 decreases with decreasing E because the line around ω_2 becomes narrower and its contribution to the energy at ω_1 is reducing.

VI. CONCLUSION

The propagation of rays of inertial waves in a closed container is governed by a reflection law which allows rays to converge to attractors after multiple reflections. In a spherical shell, two attractors can coexist at the same excitation frequency. In this respect, spherical shells are different from the containers considered in the oceanographic context by Maas and Lam [1].

Ray attractors have surprisingly little influence on global quantities like the energy contained in driven motion despite the direct bearing of ray geometry on flow structures. In an earthlike shell with $r_i/r_0=0.35$, resonant frequencies are within a few percent of the frequencies of the corresponding eigenmodes of a full sphere [14], a geometry in which no ray attractors exist at all.

The simulated flows have revealed patterns of internal shear layers which coincide with ray attractors of small period, but shear layers on a ''trapped'' attractor confined to the equatorial region have never been observed. On the other hand, shear layers may appear on closed cycles which are not attractors. The special role played by critical latitudes in rotating fluids also leads to patterns in which shear layers emanate from critical latitudes but dissipate away after several reflections before they reach an attractor predicted by ray theory. It remains an open question whether internal layers at all ω are eventually confined to the corresponding attractors for low enough Ekman numbers. This behavior would be expected if rays are an increasingly better approximation for internal layers with decreasing E. Figure 8 suggests that this may not be the case.

[1] L. R. M. Maas and F.-P. A. Lam, J. Fluid Mech. **300**, 1 (1995).
[2] L. R. M. Maas, D. Benielli, J. Sommeria, and F.-P. A. Lam, Nature (London) **388**, 557 (1997).
[3] F. P. Bretherton, Tellus **16**, 181 (1964).
[4] M. Israeli, Stud. Appl. Math. **51**, 219 (1972).
[5] K. D. Aldridge and A. Toomre, J. Fluid Mech. **37**, 307 (1969).
[6] K. D. Aldridge, Geophys. J. R. Astron. Soc. **42**, 337 (1975).
[7] K. D. Aldridge and L. I. Lumb, Nature (London) **325**, 421 (1987).
[8] K. K. Zhang, J. Fluid Mech. **268**, 211 (1994).
[9] K. K. Zhang, J. Fluid Mech. **284**, 239 (1995).
[10] R. R. Kerswell, Geophys. Astrophys. Fluid Dyn. **72**, 107 (1993).
[11] M. Rieutord and L. Valdettaro, J. Fluid Mech. **341**, 77 (1997).
[12] A. Tilgner, Int. J. Numer. Methods Fluids (to be published).
[13] H. P. Greenspan, *The Theory of Rotating Fluids* (Cambridge University Press, Cambridge, 1969).
[14] M. Rieutord, Phys. Earth Planet. Inter. **91**, 41 (1995).
[15] R. Hollerbach and R. R. Kerswell, J. Fluid Mech. **298**, 327 (1995).
[16] A. Tilgner, J. Fluid. Mech. **379**, 303 (1999).
[17] P. Fotheringham and R. Hollerbach, Geophys. Astrophys. Fluid Dynamics **89**, 23 (1998).
[18] K. Stewartson and J. A. Rickard, J. Fluid Mech. **35**, 759 (1969).
[19] M. Rieutord, Geophys. Astrophys. Fluid Dyn. **59**, 185 (1991).